BIOCHEMISTRY
including biophysical chemistry & molecular biology
Article

Biochemistry **2009,** *48,* 10793–10802 10793
DOI: 10.1021/bi901074h

Toward Understanding the Function of the Universally Conserved GTPase HflX from *Escherichia coli*: A Kinetic Approach[†]

Michael J. Shields,[‡] Jeffrey J. Fischer,[‡] and Hans-Joachim Wieden*

Department of Chemistry and Biochemistry, University of Lethbridge, Lethbridge, Alberta, Canada [‡]*Authors contributed equally to this work.*

Received June 24, 2009; Revised Manuscript Received September 29, 2009

ABSTRACT: Protein synthesis is a highly conserved process in all living cells involving several members of the translation factor (TRAFAC) class of P-loop GTPases, which play essential roles during translation. The universally conserved GTPase HflX has previously been shown to associate with the 50S ribosomal subunit, as well as to bind and hydrolyze both GTP and ATP. In an effort to elucidate the cellular function of HflX, we have determined the kinetic parameters governing the interaction between HflX and these two purine nucleotides using fluorescence-based steady-state and pre-steady-state techniques. On the basis of these, we demonstrate that the GTPase and ATPase activity of HflX is stimulated by 50S and 70S ribosomal particles. However, given cellular concentrations of the two purine nucleotides, approximately 80% of HflX will be bound to guanine nucleotides, indicating that HflX may function as a guanine nucleotide dependent enzyme in vivo. Using a highly purified reconstituted in vitro translation system, we show that the GTPase activity of HflX is also stimulated by poly(U) programmed 70S ribosomes and that the ribosome-dependent GTPase stimulation is specifically inhibited by the antibiotic chloramphenicol, which binds to the large ribosomal subunit, but not by kanamycin, an aminoglycoside targeting the small ribosomal subunit.

The GTPases of the P-loop[1] family are highly conserved proteins that function as molecular switches, modulating a wide variety of cellular processes in response to conformational changes induced by hydrolysis of GTP. Structurally, these proteins contain the α/β G-domain, consisting of the following conserved sequence motifs: the G1 motif (or P-loop), consensus $GX_4GK(S/T)$, which is responsible for interacting with the α- and β-phosphates of nucleotide di- and triphosphates; the G2 variable effector loop (DX_nT); the G3 motif (DX_2G), which interacts with the γ-phosphate of nucleotide triphosphates; and the G4 motif (NKXD), which conveys specificity for guanine nucleotides through hydrogen bonding to the base (*1*). Functionally, many of these GTPases have been linked to roles in tRNA modification, DNA replication, signal transduction, and protein synthesis (*2*, *3*).

Guanine nucleotide binding proteins exist in three different conformations: the transient *apo* state can bind to either GTP or GDP under cellular concentrations of guanine nucleotides. Binding to GTP causes the protein to adopt a functional GTP-bound "active" state (*1*). Upon hydrolysis of GTP, the protein reverts to its "inactive", GDP-bound state. GDP then dissociates, and the cycle continues. The conversions between these states are often catalyzed by regulatory proteins, which affect the kinetics of the interaction between the GTPase and guanine nucleotides. These regulators include guanine nucleotide exchange factors (GEFs), which catalyze the release of bound GDP, which in turn promotes GTP binding; GTPase activating proteins (GAPs), which stimulate the low intrinsic GTPase activity of the protein; and guanine nucleotide dissociation inhibitors (GDIs), associated with regulating members of the small G-protein superfamily, such as Rab and Rho in eukaryotes (*4*−*6*), which inhibit nucleotide dissociation as a regulatory mechanism.

A core group of eight universally conserved GTPases found in all domains of life has been identified and includes elongation factors (EFs) Tu and G, initiation factor (IF) 2, protein secretion factors Ffh and FtsY, and the relatively poorly characterized proteins YihA, YchF, and HflX (*2*). Additional GTPases, conserved in prokaryotes and eukaryotes but not archaea, include Obg, EngA, and Era (*2*). The protein HflX, a member of the Obg-HflX superfamily, was initially linked to a role in determining the lysis-lysogeny decision of bacteria infected with bacteriophage lambda (*7*, *8*). However, recent data has shown that HflX from *Chlamydophila pneumonia* possesses a slow intrinsic GTPase activity and cofractionates with *Escherichia coli* 50S ribosomal subunits, suggesting the protein may have a role in protein synthesis (*9*). *E. coli* HflX has been shown to possess both GTPase and ATPase activity; surprisingly, only the GTPase activity was shown to be stimulated by the 50S ribosomal subunit (*10*). Thus, HflX represents the second member of the Obg-HflX superfamily after YchF which demonstrates both

[†]This work was supported by the National Science and Engineering Research Council (NSERC), Canada Foundation for Innovation (CFI), and the Canadian Institutes for Health Research (CIHR).

*To whom correspondence should be addressed. Address: 4401 University Drive, Lethbridge, Alberta T1K 3M4. Phone: (403)-329-2303; fax: (403)-329-2057; e-mail: hj.wieden@uleth.ca.

[1]Abbreviations: TRAFAC, translation factor; P-loop, phosphate-binding loop; GEF, guanine nucleotide exchange factor; GAP, GTPase activating protein; GDI, guanine nucleotide dissociation inhibitor; EF, elongation factor; IF, initiation factor; mant, 2′(3′)-*O*-(*N*-methylanthraniloyl); X-gal, 5-bromo-4-chloro-3-indolyl-β-D-galactopyranoside; IPTG, isopropyl-β-D-galactopyranoside; PMSF, phenylmethylsulfonylfluoride; MWCO, molecular weight cutoff; PK, pyruvate kinase; PEP, phosphoenolpyruvate; K_D, equilibrium dissociation constant; FRET, fluorescence resonance energy transfer; IC_{50}, 50% inhibitory concentration.

© 2009 American Chemical Society
Published on Web 10/13/2009

GTPase and ATPase activity (*11*, *12*), despite the presence of the G4 specificity motif. Additionally, HflX interacts with both 16S and 23S rRNA in a nucleotide-dependent manner, as shown by gel shift assays (*10*). Recently, Dutta and colleagues confirmed that HflX binds and hydrolyzes both purine nucleotides, and also discounted suggested roles for HflX in the bacterial lysis/lysogeny decision and transposition (*13*). However, no detailed information about the kinetic parameters governing these interactions is available to date, information pivotal to unraveling the functional mechanism of HflX action.

In this work, we report for the first time the detailed analysis of the purine nucleotide binding properties of HflX as studied by equilibrium and pre-steady-state fluorescence techniques. Thereby we confirm that HflX binds both adenine and guanine nucleotides, with a preference for guanine nucleotides. Using fluorescent analogues of guanine nucleotides (mant-GDP and mant-GTP), we have determined the elemental rate constants governing the interaction between HflX and the respective mant-guanine nucleotides using the stopped-flow technique. On the basis of our data, we have established appropriate conditions to study the NTPase activity of HflX. We demonstrate that the NTPase activity of HflX is not only stimulated by 50S ribosomal subunits, but also to a similar extent by empty 70S ribosomes as well as ribosome complexes containing the synthetic mRNA analogue poly(U) and deacylated $tRNA^{Phe}$ in the ribosomal P-site. Although an interaction between 16S/23S rRNA and HflX has been reported by Jain and colleagues (*10*), the NTPase activity of HflX is not significantly stimulated by 30S ribosomal subunits. On the basis of our pre-steady-state analysis and nucleotide hydrolysis data, we propose a kinetic scheme for HflX with respect to the GTPase cycle as described by Bourne and colleagues (*1*). We also demonstrate that the 70S ribosome stimulated GTPase activity is inhibited by the antibiotic chloramphenicol, but not by kanamycin. Chloramphenicol binds to the 50S ribosomal subunit at 23S rRNA bases A2451 and A2452, near the peptidyl transferase center (*14*), while kanamycin interacts at a site common to aminoglycoside antibiotics on the 30S ribosomal subunit at 16S rRNA bases A1408, G1419, and G1494, near the mRNA decoding center on the 70S ribosome (*15*−*17*).

EXPERIMENTAL PROCEDURES

Materials. All chemicals were obtained from VWR, Sigma, or Invitrogen, unless otherwise specified. Restriction enzymes were from Fermentas; all other enzymes were purchased as described in the following sections. PCR primers, nucleotides, and mant-nucleotides were purchased from Invitrogen (mant nucleotides ≥ 94% purity based on manufacturers specifications). Radiochemicals were purchased from Perkin-Elmer. Small-scale plasmid preparations were performed according to the manufacturer's specifications (EZ spin column plasmid DNA kit, BioBasic). Antibiotics were from BioBasic.

Molecular Biology. Open reading frame *hflX* was PCR amplified from *E. coli* genomic DNA in a reaction catalyzed by Phusion polymerase (Finnzymes) using primers 5′-CTA TTT AAG AGG GGT TAT ACA TAT GTT-3′ and 5′-AAG CTT CGC CGT TAG ATC AGG TA-3′, where underlined nucleotides respectively denote *Nde*I and *Hind*III restriction sites engineered into the primers. The resulting 1.3 kb PCR product was ligated (T4 DNA ligase, Invitrogen) into *Sma*I digested pUC19. The ligation mixture was transformed into subcloning efficiency *E. coli* DH5α cells (Invitrogen), which were then grown at 37 °C on LB-agar plates supplemented with 50 μg/mL ampicillin and 50 μg/mL X-gal (Rose Scientific). On the basis of blue-white selection and restriction analysis, cells containing recombinant plasmids were further propagated for plasmid isolation. The open reading frame was excised from pUC*hflX* using *Nde*I and *Hind*III restriction endonucleases and ligated into similarly digested pET28a to create plasmid pET*hflX*. *E. coli* strain DH5α was used for propagation. All recombinant plasmids were characterized by DNA sequencing (Macrogen DNA Sequencing Services) to confirm sequence, gene orientation, and reading frame.

Expression and Detection. The plasmid pET*hflX* was transformed into *E. coli* strain BL21-DE3 (Invitrogen) for expression of recombinant His-tagged HflX. Cells were grown at 37 °C in LB media supplemented with 50 μg/mL kanamycin and induced at an $OD_{600} \sim 0.6$ with IPTG (final concentration of 1 mM). Cells were grown for an additional 3 h until the late logarithmic growth phase was reached, and harvested by centrifugation at 5000*g*. Cells were flash frozen and stored at −80 °C prior to use.

To monitor protein expression levels, small culture samples were taken and lysed in 8 M urea. Cleared cell lysates were then analyzed using 12% SDS−PAGE at 200 V for 55 min. Gels were stained with Coomassie blue; all other SDS−PAGEs were performed in a similar manner.

Protein Purification. Cells were resuspended in 7 mL/g of cells buffer A (50 mM Tris-Cl pH 8.0 at 4 °C, 60 mM NH_4Cl, 300 mM KCl, 7 mM $MgCl_2$, 7 mM β-mercaptoethanol, 10 mM imidazole, 15% v/v glycerol, 50 μM GDP, 1 mM PMSF) and opened by incubation on ice with lysozyme (1 mg/mL final concentration) for 30 min. Sodium deoxycholate (12.5 mg/g of cells) was added, followed by incubation on ice until the viscosity of the solution increased. The solution was then sonicated until the viscosity of the solution decreased again, and subsequently centrifuged for 30 min at 3000*g* (4 °C) to remove cell debris. The supernatant was further centrifuged for 45 min at 30000*g* (4 °C) to obtain cleared cell lysate.

The resulting cleared lysate was applied to a 10 mL Ni^{2+} sepharose column (GE Healthcare). The column was washed with 50 column volumes buffer A, followed by a similar wash with buffer B (buffer A with 20 mM imidazole, lacking GDP). Recombinant His-tagged HflX was eluted from the column in several steps (90% column volume each) using buffer E (buffer A with 300 mM imidazole, lacking GDP). Fractions containing HflX were pooled and concentrated using a Vivaspin 20 (10 000 MWCO, Sartorius). The protein was further purified by size exclusion chromatography using Superdex-75 (XK26/100 column, GE Healthcare) equilibrated in buffer C (50 mM Tris-Cl pH 7.5 at 4 °C, 70 mM NH_4Cl, 300 mM KCl, 7 mM $MgCl_2$). Fractions containing pure HflX were pooled and concentrated; protein concentration was determined photometrically at 280 nm using a molar extinction coefficient of 32555 $M^{-1}cm^{-1}$ (calculated using the software ProtParam (*18*)) and using the BioRad microassay. Protein samples were aliquoted, flash frozen, and stored at −80 °C prior to use.

Purification of Ribosomes and Complex Formation. Vacant ribosomes were purified from *E. coli* MRE600 cells essentially as described in ref *19*, but using a Ti 45 rotor rather than a Ti 50.2 rotor. Ribosomal complexes were programmed with poly(U) mRNA and P-site $tRNA^{Phe}$ (both from Sigma) similar to previous literature (*20*). Briefly, complexes were formed

by incubating 70S ribosomes (60 pmol) with 1.3 molar excess of $tRNA^{Phe}$ and 1 mg/mL poly(U) (determined by absorbance at 260 nm) in buffer $TAKM_7$ (50 mM Tris-Cl pH 7.5 at room temperature, 70 mM NH_4Cl, 30 mM KCl, 7 mM $MgCl_2$) at 37 °C for 15 min.

Fluorescence Techniques. To determine nucleotide binding affinities, fluorescence measurements were performed using a Varian Cary Eclipse fluorescence spectrophotometer. The intrinsic tryptophan fluorescence of HflX (four residues) was excited at 280 nm in a 0.3 × 0.3 cm quartz cuvette (Starna) at room temperature. Fluorescence measurements were carried out using 1 μM HflX in buffer $TAKM_7$, and increasing amounts of the respective nucleotide were added. Fluorescence was monitored from 305 to 450 nm through 5 nm slits for titrations with adenine and guanine nucleotides, and from 305 to 605 nm for titrations with respective mant-nucleotides. Changes in fluorescence were corrected for dilution and plotted as a function of nucleotide concentration at 338 nm for nucleotide and mant-nucleotide titrations. Fluorescence signals due to the presence of protein and nucleotide individually were subtracted from the overall fluorescence of the system. Fluorescence changes (ΔFl) plotted against nucleotide concentration ([nt]) were fitted to a quadratic function (eq 1), with respect to the initial (Fl_0) and maximum (Fl_{max}) fluorescence to determine the dissociation constant (K_D) for each nucleotide or fluorescent derivative using the software TableCurve (Jandel Scientific). Additional variables for total protein concentration ([P]) and signal amplitude ($B = Fl_{max} - Fl_0$) were accounted for (*21*). Fluorescence signals were normalized prior to fitting.

$$\Delta Fl = 0.5(B/[P])(K_D + [P] + [nt] - ((K_D + [P] + [nt])^2 - 4[P][nt])^{1/2}) \quad (1)$$

The pre-steady-state kinetics of mant-nucleotide dissociation and association were determined using a KinTek SF-2004 Stopped-flow apparatus. Rate constants for the bimolecular association of mant-GTP and mant-GDP (k_1 and k_3 in Scheme 1, respectively) were determined by rapidly mixing 25 μL of HflX (2 μM, nucleotide free) with 25 μL of varying concentrations of mant-nucleotides at 20 °C in $TAKM_7$. Tryptophan residues were excited at 280 nm and fluorescence emission from the mant group was monitored through LG-400-F cutoff filters (NewPort). As only single-exponential time courses were observed, the data were treated on the basis of a one-step binding model, HflX + mant-nt ↔ HflX·mant-nt, and analyzed by exponential fitting (eq 2; with the characteristic apparent rate constant k_{app}, A for signal amplitude, Fl for the fluorescence at time t, and Fl_∞ for the final fluorescence signal) to determine the value of k_{app} for each titration point.

$$Fl = Fl_\infty + A \times \exp(-k_{app}t) \quad (2)$$

The obtained apparent rate constants were plotted as a function of nucleotide concentration; the slope of this function provided the association rate constants (k_1 and k_3 according to Scheme 1). The y-axis intercept provided estimated k_{-1} and k_{-3} for mant-GTP and mant-GDP dissociation, respectively.

To determine the rate constants for dissociation of mant-GTP and mant-GDP (k_{-1} and k_{-3} respectively), 1 μM HflX was incubated with 30 μM mant-nucleotide for 15 min at 37 °C (in $TAKM_7$). Experiments were then performed by rapidly mixing 25 μL of HflX·mant-nucleotide with 25 μL of 300 μM nucleotide (no fluorescent label) at 20 °C in $TAKM_7$. Again, only single-exponential fluorescence time courses were observed and the resulting fluorescence signal was therefore fitted with an exponential decay function (eq 2, with the characteristic apparent rate constant k_{app} corresponding to the rate of nucleotide dissociation). Rate constants for mant-nucleotide dissociation from HflX were also calculated from the respective K_D values and k_1/k_3 rate constants for comparison. Similar experiments were performed for mant-adenine nucleotides.

Scheme 1: Minimal Kinetic Mechanism Describing the Interaction between HflX and Guanine Nucleotides

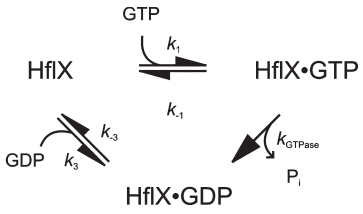

Nucleotide Hydrolysis Assays. Hydrolysis of GTP and ATP by HflX was monitored by determining the release of $^{32}P_i$ from [γ-^{32}P]GTP and [γ-^{32}P]ATP. Nucleotide charging solution (radioactive nucleotide at ~100 dpm/pmol, 0.25 μg/μL pyruvate kinase (PK), 3 mM phosphoenolpyruvate (PEP)) and HflX-charging solution (15 μM HflX, 0.25 μg/μL PK, 3 mM PEP) were incubated at 37 °C for 15 min to catalyze nucleotide triphosphate formation from the diphosphate form and to prevent inhibition of multiple turnover experiments by diphosphates. Hydrolysis assays were carried out in buffer $TAKM_7$. Reaction volumes were 60 μL and contained 1 μM HflX, 125 μM radiolabeled nucleotide solution, and 1 μM 70S ribosomes, 50S subunits, or 0.5 μM 30S ribosomal subunits. For antibiotic titrations, the appropriate concentration of antibiotic was also added. Five microliters samples were removed at different time points and quenched in 50 μL 1 M $HClO_4$ with 3 mM K_2HPO_4.

Following the addition of 300 μL 20 mM Na_2MoO_4 and 400 μL isopropyl acetate, samples were mixed for ~30 s and centrifuged at 15800g for 5 min. $^{32}P_i$ was extracted as a phosphate-molybdate complex in the organic phase, added to 2 mL of EcoLite scintillation cocktail (EcoLite, MP Biomedical), and counted in a Perkin-Elmer Tri-Carb 2800TR liquid scintillation analyzer. Background radioactivity due to NTP hydrolysis by ribosomes or self-hydrolysis was subtracted; concentration of $^{32}P_i$ released was calculated and plotted.

The apparent rate of nucleotide hydrolysis by HflX, alone or in the presence of ribosomes and antibiotics, was calculated from fitting the initial linear phase of multiple turnover experiments to a linear equation, where the slope of the fit is the apparent rate of nucleotide hydrolysis, k_{app}.

RESULTS

Equilibrium Analysis of HflX Interacting with Nucleotides. On the basis of the analysis of available primary sequences from different organisms, Jain and colleagues generated truncated versions of HflX deleting single domains (The predicted domain arrangement is summarized in Figure 1) and demonstrated that all three domains are required for association with the 50S ribosomal subunit (*10*). Within the G domain, the essential elements required for nucleotide binding and specificity are indeed conserved among the universally conserved GTPases, with the exception of the G4 motif of YchF. Despite the conservation of these motifs, previous studies on HflX's purine nucleotide specificity are contradictory. Results reported by

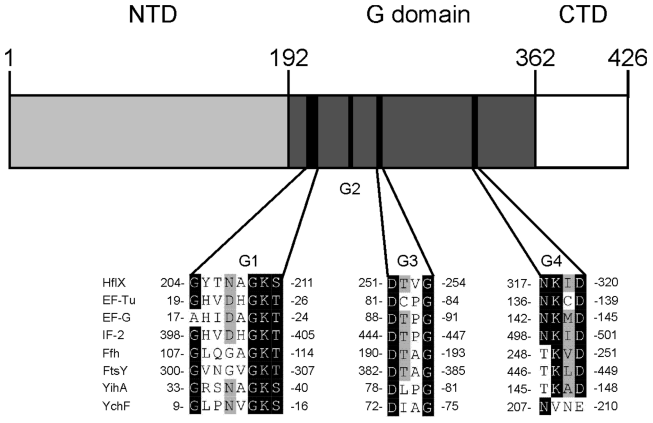

FIGURE 1: Structural features of HflX. The protein consists of three domains: an N-terminal domain (light gray), a central G domain (dark gray), and a short C-terminal domain (white). The G1, G3, and G4 motifs are conserved with other members of the universally conserved GTPases (black).

Polkinghorne et al. based on competition assays support the annotation that HflX from *C. pneumoniae* is specific for guanine nucleotides (*9*), while results by Jain et al. and Dutta et al. indicate that HflX from *E. coli* binds and hydrolyzes ATP and GTP (*10*, *13*). Since the experimental approaches used in these previous studies did not take into account a wide range of affinities for the different nucleotides, they might not have been sensitive enough to detect the interaction. Therefore, a quantitative kinetic description of the interaction with the two purine nucleotides is crucial for understanding their functional importance. We have used equilibrium fluorescence spectroscopy measurements to study the nucleotide binding properties of purified *E. coli* HflX. Guanine and adenine di- and triphosphates were added into HflX solutions, and changes in tryptophan fluorescence were monitored. The addition of increasing amounts of guanine nucleotides resulted in a decrease in tryptophan fluorescence ($\lambda_{emission,max} = \sim 338$ nm, Figure 2A,B). Similar results were obtained for titrations of the protein with adenine nucleotides (data not shown). From these titrations the equilibrium dissociation constant (K_D) was determined by fitting the concentration dependence of tryptophan fluorescence to a quadratic function (Experimental Procedures). These results not only reveal a preference for nucleotide diphosphates (K_D values of 3.2 ± 0.4 μM and 12 ± 1 μM for GDP and ADP respectively) compared to nucleotide triphosphates (K_D values of 187 ± 7 μM and 362 ± 20 μM for GTP and ATP respectively), but also a slightly higher affinity for guanine nucleotides.

In order to improve the signal-to-noise ratio for the pre-steady-state analysis, we have used fluorescence resonance energy transfer (FRET) between the tryptophan residues in HflX and the respective mant-labeled nucleotides. We therefore first determined the equilibrium binding constants of HflX to several mant-nucleotide derivatives, a modification that has previously been successfully used in the pre-steady-state analysis of other G-proteins such as EF-Tu (*22*). Upon excitation of tryptophan residues in HflX, FRET to the mant group of mant-GTP and GDP was observed, as reflected by a decrease in tryptophan fluorescence (Figure 2C,D) and an increase in mant fluorescence ($\lambda_{emission,max} = \sim 450$ nm). Changes in the relative fluorescence at the tryptophan emission wavelength (338 nm) as a function of mant-nucleotide concentration revealed comparable, but slightly higher binding affinities for mant-nucleotides when compared to the nonfluorescent nucleotides (0.8 ± 0.1 μM and 48 ± 4 μM for mant-GDP and mant-GTP respectively). Similar trends were observed for titrations of HflX with mant-adenine nucleotides (8.1 ± 1.9 μM and 87 ± 19 μM for mant-ADP and mant-ATP, respectively). However, in these titrations the observed change in mant fluorescence was significantly smaller when compared to the guanine nucleotide derivatives (data not shown). The equilibrium binding constants for the respective nucleotides are summarized in Table 1 and are consistent with those reported for the other universally conserved GTPases (Table 2).

Pre-Steady-State Kinetic Analysis of HflX Interacting with mant-Nucleotides. On the basis of the GTPase cycle outlined by Bourne (*1*), and our observation that HflX seems to have a preference for guanine nucleotides, a minimal kinetic scheme for the interaction of HflX with guanine nucleotides is presented (Scheme 1). To study the mechanism of nucleotide interaction with HflX, we performed a rapid kinetics analysis using the stopped-flow technique observing FRET between HflX tryptophan residues and the mant group of mant-nucleotides over time. This approach has been successfully used previously to study nucleotide binding properties of a variety of other GTPases such as EF-Tu and IF-2 (*22*−*24*). Upon rapid mixing of varying concentrations of mant-GDP with HflX, a fast increase in fluorescence of the mant group due to FRET, reflecting the binding of mant-GDP, was observed that was dependent on the nucleotide concentration (Figure 3A). As only single exponential time courses were observed, these data were treated as a one-step binding model, similar to that of EF-Tu binding to mant nucleotides (*22*). The bimolecular association constant for binding of mant-GDP to HflX (k_3) was obtained from the slope of the linear concentration dependence of k_{app} (Figure 3B), and was determined to be $9.7 \pm 0.6 \times 10^5$ M^{-1} s^{-1}. A similar experiment examining the interaction between mant-GTP and HflX yielded a value of $k_1 = 6.4 \pm 0.3 \times 10^4$ $M^{-1}s^{-1}$.

To measure the rate of nucleotide dissociation (k_{-3}), HflX was incubated with a 30-fold excess of mant-GDP; the HflX·mant-GDP complex was then rapidly mixed with an excess of nonfluorescent GDP (300-fold excess). The change in fluorescence reflecting the mant-GDP dissociation was monitored (Figure 3C), and k_{-3} was determined by fitting the observed fluorescence change to a single-phase exponential function. The value for k_{-3} was determined to be 2.6 ± 0.2 s^{-1}. This value is in agreement with the *y*-axis intercept of the concentration dependence of the association rate (k_{app}) used to determine k_3 ($k_{-3} = 2.2 \pm 0.3$ s^{-1}). Because of the low intrinsic NTPase activity of HflX, k_{-1} was determined in a similar fashion. Values for k_{-1} were determined as 2.1 ± 0.1 s^{-1} from dissociation experiments and 1.9 ± 0.1 s^{-1} from the plot of k_{app} dependence of k_1. A summary of all determined rate constants is given in Table 3.

Interestingly, when similar experiments were performed with mant-derivatives of adenine nucleotides, no changes in the mant fluorescence signal were observed (data not shown). This was surprising since equilibrium binding data demonstrated FRET between the intrinsic tryptophan residues of HflX and the mant group of mant-adenine nucleotides. However, the mant-fluorescence signal was significantly smaller for the mant-adenine nucleotide titrations compared to the respective mant-guanine nucleotide titrations, and possibly too small to be detected in stopped-flow assays. Since FRET is very sensitive to variations in distance between the fluorescence donor and acceptor dyes, these

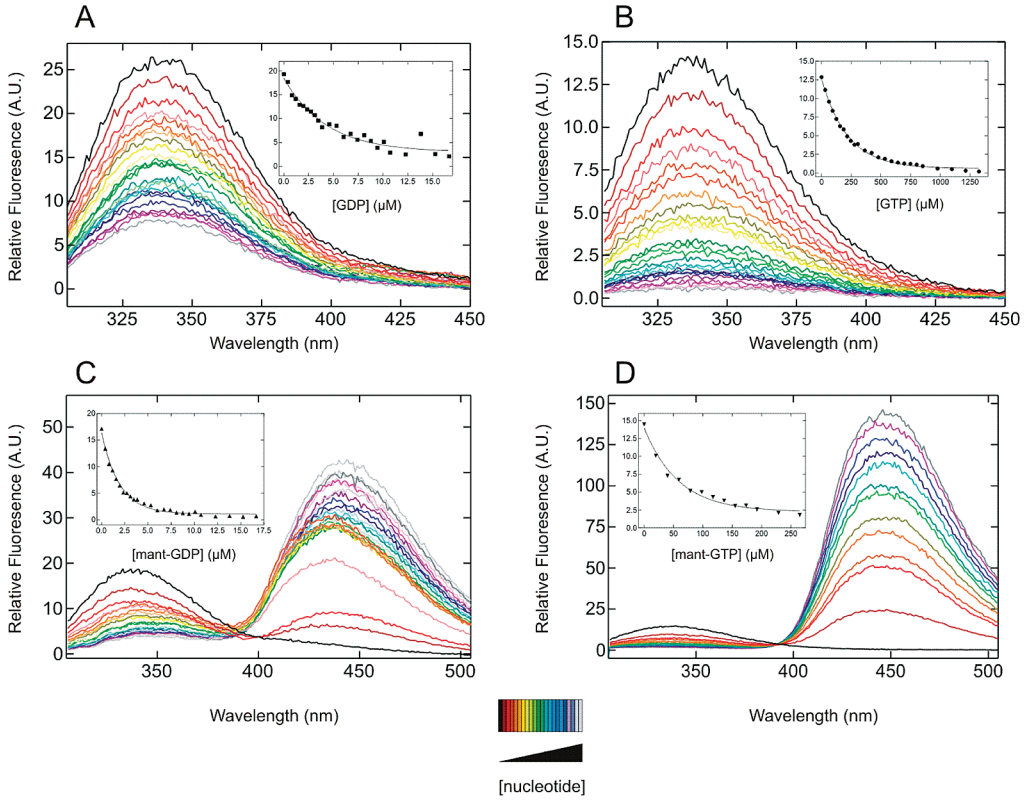

FIGURE 2: Equilibrium fluorescence titration of HflX with guanine nucleotides. HflX was titrated with increasing amounts of (A) GDP, (B) GTP, (C) mant-GDP, and (D) mant-GTP according to the color scheme provided (bottom). Insets show the nucleotide concentration dependence of the obtained tryptophan fluorescence signal (at 338 nm) used to determine K_D values.

Table 1: Dissociation Constants (K_D) Governing the Interaction between HflX and Purine Nucleotides

nucleotide	parameter, signal	description	value (μM)
GTP	K_D, HflX intrinsic tryptophan	dissociation constant	187 ± 7
GDP	K_D, HflX intrinsic tryptophan	dissociation constant	3.2 ± 0.4
mant-GTP	K_D, HflX intrinsic tryptophan	dissociation constant	48 ± 4
mant-GTP	K_D, calculated from k_{-1}/k_1	comparison to $K_{Dmant\text{-}GTP}$	30 ± 1
mant-GDP	K_D, HflX intrinsic tryptophan	dissociation constant	0.8 ± 0.1
mant-GDP	K_D, calculated from k_{-3}/k_3	comparison to $K_{Dmant\text{-}GDP}$	2.7 ± 0.2
ATP	K_D, HflX intrinsic tryptophan	dissociation constant	362 ± 20
ADP	K_D, HflX intrinsic tryptophan	dissociation constant	12 ± 1
mant-ATP	K_D, HflX intrinsic tryptophan	dissociation constant	87 ± 19
mant-ADP	K_D, HflX intrinsic tryptophan	dissociation constant	8.1 ± 1.9

Table 2: Dissociation Constants (K_D) Governing the Interaction between GTP/GDP and the Universally Conserved GTPases

classification	protein	K_D, GTP	K_D, GDP	ratio	reference
translation factors	EF-Tu	60 nM	1 nM	60	*23*
	EF-G	7 μM	17 μM	0.41	*21*
	IF-2	140 μM	13 μM	11	*37*
protein secretion factors	FtsY	14 μM	26 μM	0.54	*38*
	Ffh	0.3 μM	0.2 μM	1.5	*38*
Era group	YihA	3 μM	27 μM	0.11	*39*
Obg group	YchF	5 μM	~15 μM[a]	0.33	*40*
	HflX	187 μM	3.2 μM	58	this study

[a] A. Altamirano, personal communication.

observations might reflect a slightly different position of the guanine compared to the adenine nucleotides relative to the donor tryptophan.

NTPase Activity of HflX in the Presence of Ribosomes and Ribosomal Subunits. The GTPase activity of HflX was recently reported to be specifically stimulated by 50S ribosomal subunits (*10*). Here we demonstrate that the intrinsic GTPase activity of HflX (Figure 4A) is very slow ($k_{GTPase} = 8.4 \pm 0.1 \times 10^{-4}$ μM s^{-1}) and can be stimulated ~ 1000 fold by 50S ribosomal subunits ($k_{GTPase,50S} = 0.19 \pm 0.01$ μM s^{-1}) as well as by empty 70S ribosomal complexes ($k_{GTPase,70S}$ 0.24 ± 0.01 μM s^{-1}). In an effort to elucidate the functional state in which HflX interacts with the ribosome, the GTPase activity of HflX was examined in the presence of ribosome complexes containing poly(U) as the message and $tRNA^{Phe}$ in the P site. Programming and P-site occupancy had little effect on the ribosome-stimulated GTPase activity of HflX (Figure 4B, $k_{GTPase,p(U)70S} = 0.17 \pm 0.01$ μM s^{-1}).

Surprisingly, previous studies indicate that although *E. coli* HflX is able to bind both purine nucleotides, only the GTP

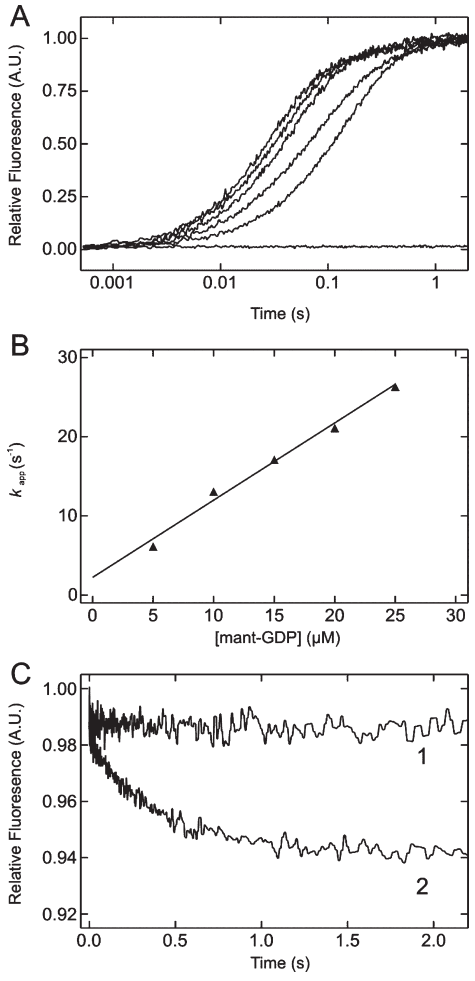

FIGURE 3: Rapid kinetic analysis of the interaction of mant-GDP with HflX. (A) Time courses of mant-GDP binding to HflX measured by FRET. From right to left: 5, 10, 15, 20, and 25 μM mant-GDP, baseline (control without nucleotide). (B) Concentration dependence of k_{app}. Values of k_{app} were calculated as described in Experimental Procedures; standard deviations range from 1.4 to 3.2%. From the slope of this plot, the association rate constant k_3 ($9.7 \pm 0.6 \times 10^5\ M^{-1}\ s^{-1}$) was calculated. The y intercept corresponds to k_{-3} ($2.2 \pm 0.3\ s^{-1}$). (C) Determination of the rate constant of mant-GDP dissociation k_{-3} from HflX. (1) Nucleotide free control and (2) dissociation of mant-GDP from HflX. All traces were normalized with respect to the initial fluorescence of the system.

hydrolysis activity but not the ATP hydrolysis activity could be stimulated by 50S ribosomal subunits (*10*). This might be explained by the significantly different affinities for the nucleotide diphosphates and triphosphates (between 30- and 58-fold difference) determined in this study; that is, the experimental conditions might favor binding of the diphosphate in the first round of catalysis, thereby preventing binding and hydrolysis of further triphosphates. To overcome this, we used pyruvate kinase and phosphoenolpyruvate to convert all nucleotide present into the triphosphate form. On the basis of the equilibrium dissociation constant of GTP (around 190 μM), we performed the hydrolysis experiments in the presence of 125 μM radiolabeled nucleotide, ensuring efficient binding to the enzyme. Using this optimized assay condition, we are able to demonstrate that both the HflX GTP and ATP hydrolysis activity can be stimulated by both 70S ribosomes and 50S ribosomal subunits. The observed stimulated multiple turnover ATP hydrolysis rates (Figure 4C: $k_{ATPase,70S} = 1.4 \pm 0.4 \times 10^{-2}\ \mu M\ s^{-1}$; $k_{ATPase,50S} = 2.3 \pm 0.4 \times 10^{-2}\ \mu M\ s^{-1}$) are significantly slower compared to the respective GTPase activity ($k_{GTPase,70S}$ $0.24 \pm 0.01\ \mu M\ s^{-1}$; $k_{GTPase,50S} = 0.19 \pm 0.01\ \mu M\ s^{-1}$) of HflX, which is consistent with the lower affinity of HflX for ATP (2−3 times lower than GTP, Table 3).

Effect of Translation-Inhibiting Antibiotics on the Ribosome Stimulated GTPase of HflX. In order to address the question if HflX specifically interacts with the 50S ribosomal subunit, we assayed the effect of two antibiotics that inhibit protein synthesis by binding to different subunits of the ribosome on the rate of ribosome-stimulated GTP hydrolysis. To this effect, we determined the apparent rate of ribosome stimulated GTP hydrolysis by HflX in the presence of increasing concentrations of chloramphenicol and kanamycin, which interact specifically with the 50S and 30S ribosomal subunit, respectively. While kanamycin did not show any effect on the rate of GTP hydrolysis (Figure 5A), in the presence of chloramphenicol the apparent rate of ribosome stimulated GTP hydrolysis by HflX decreased significantly with increasing concentration of the antibiotic (Figure 5B,C). On the basis of this effect, 50% inhibitory concentrations (IC_{50}) of chloramphenicol were calculated as 200 μM for both 70S ribosomes and 50S ribosomal subunits.

DISCUSSION

HflX is a member of the Obg-HflX superfamily of conserved TRAFAC GTPases (*25*). The members of this superfamily include Obg (also CtgA or YhbZ), YchF, and HflX (*2*), and have been implicated in ribosome biogenesis and regulation of translation. For example, Obg from *E. coli* and *Vibrio harveyi* has been shown to associate with the 50S ribosomal subunit, and has an essential role in its maturation (*26*, *27*). On the basis of the kinetic parameters reported in this study we are now making progress toward a detailed understanding of the molecular mechanism of HflX's function, one of the eight universally conserved GTPases found in all domains of life. HflX is particularly interesting since it represents the second member of these conserved GTPases, after YchF, that binds both purine nucleotides (*12*). This is surprising, since the G4 motif (NKID) found in HflX from *E. coli* corresponds well with the consensus sequence NKXD motif determining nucleotide specificity in P-loop GTPases. In contrast, YchF from *E. coli* preferentially binds adenine nucleotides and contains an altered G4 sequence (NVNE), which, supported by the available X-ray structures, is likely to be responsible for the observed change in specificity. The equilibrium binding constants for GTP and ATP (187 and 362 μM respectively) reported here for HflX support the previously observed lack of nucleotide specificity (*10*, *13*), but also show a slight preference for guanine nucleotides. Adenine nucleotides are in ~3-fold excess over guanine nucleotides in vivo and cellular concentrations of purine nucleotides are ~10−20-fold higher for the triphosphate form compared to the diphosphate form (GTP = 0.9−1.7 mM/GDP = 0.1−0.2 mM and ATP = 2.5−3.6 mM/ADP = 0.13−0.25 mM) (*28*, *29*). Therefore, approximately 19% of HflX will be bound to the triphosphates (roughly equal amounts to GTP and ATP), 80% to the diphosphates (70% to GDP and 10% to ADP) and only 1% in the nucleotide free form. This in turn also indicates that almost 80% of the cellular HflX will be found in the guanine nucleotide bound form, suggesting that HflX functions as a guanine nucleotide dependent enzyme in vivo. The observation that HflX is nonessential under optimal growth conditions, based on the growth pattern of a *hflX* knockout strain (*30*), suggests to us a

Table 3: Kinetic Constants Governing the Interaction between HflX and Purine Nucleotides

nucleotide	parameter, signal	description	value
mant-GTP	k_1, FRET to mant group	mant-GTP association	$6.4 \pm 0.3 \times 10^4$ M^{-1} s^{-1}
mant-GTP	k_{-1}, FRET to mant group	mant-GTP dissociation	2.1 ± 0.1 s^{-1}
mant-GTP	k_{-1}, from k_{app} vs [mant-GTP] plot	mant-GTP dissociation	1.9 ± 0.1 s^{-1}
GTP	k_{GTPase}, hydrolysis of [γ-^{32}P]GTP	GTP hydrolysis	$8.4 \pm 0.1 \times 10^{-4}$ μM s^{-1}
GTP	$k_{GTPase,70S}$, hydrolysis of [γ-^{32}P]GTP	GTP hydrolysis, + 70S	0.24 ± 0.01 μM s^{-1}
GTP	$k_{GTPase,p(U)70S}$, hydrolysis of γ-^{32}P]GTP	GTP hydrolysis, + programmed 70S	0.17 ± 0.01 μM s^{-1}
GTP	$k_{GTPase,50S}$, hydrolysis of [γ-^{32}P]GTP	GTP hydrolysis, + 50S	0.19 ± 0.01 μM s^{-1}
GTP	$k_{GTPase,30S}$, hydrolysis of [γ-^{32}P]GTP	GTP hydrolysis, + 30S	$2.3 \pm 0.2 \times 10^{-3}$ μM s^{-1}
mant-GDP	k_3, FRET to mant group	mant-GDP association	$9.7 \pm 0.6 \times 10^5$ M^{-1} s^{-1}
mant-GDP	k_{-3}, FRET to mant group	mant-GDP dissociation	2.6 ± 0.2 s^{-1}
mant-GDP	k_{-3}, from k_{app}vs [mant-GDP] plot	mant-GDP dissociation	2.2 ± 0.3 s^{-1}
ATP	k_{ATPase}, hydrolysis of [γ-^{32}P]ATP	ATP hydrolysis	$8.0 \pm 1.6 \times 10^{-4}$ μM s^{-1}
ATP	$k_{ATPase,\ 70S}$, hydrolysis of [γ-^{32}P]ATP	ATP hydrolysis, + 70S	$1.4 \pm 0.4 \times 10^{-2}$ μM s^{-1}
ATP	$k_{ATPase,\ 50S}$, hydrolysis of [γ-^{32}P]ATP	ATP hydrolysis, + 50S	$2.3 \pm 0.4 \times 10^{-2}$ μM s^{-1}
ATP	$k_{ATPase,\ 30S}$, hydrolysis of [γ-^{32}P]ATP	ATP hydrolysis, + 30S	$3.8 \pm 3.2 \times 10^{-4}$ μM s^{-1}

role for HflX under stress conditions instead, probably by regulating either ribosome biogenesis or protein synthesis. Determining the affinity of HflX for 70S ribosomal complexes and the 50S subunit with respect to its nucleotide bound state will provide valuable information on the association of the protein with the ribosome under in vivo conditions.

The presented pre-steady-state kinetic analysis of HflX has revealed that the association rate constants for mant-GTP and GDP binding ($k_1 = 6.4 \pm 0.3 \times 10^4$ M^{-1} s^{-1} and $k_3 = 9.7 \pm 0.6 \times 10^5$ M^{-1} s^{-1}, respectively) are ~20-fold different. However, the dissociation rate constants of mant-GTP and GDP dissociation are of the same order of magnitude ($k_{-1} = 2.1 \pm 0.1$ s^{-1} and $k_{-3} = 2.6 \pm 0.2$ s^{-1}), resulting in an approximately 20-fold lower affinity for the nucleotide triphosphate compared to the respective diphosphate. These rapid nucleotide dissociation rates are also observed in Obg from *Caulobacter crescentus* (1.4 and 1.5 s^{-1} for mant-GDP and mant-GTP, respectively (*31*)) and *E. coli* (1.1 s^{-1} and 0.57 s^{-1} for mant-GDP and mant-GTP, respectively (*32*)). The relatively fast dissociation of both nucleotides from the complex will ensure the rapid turnover of the bound nucleotide, and thus no guanine nucleotide exchange factor (GEF) will be required for HflX's function. This is in contrast to the dissociation rate constants of for example EF-Tu ($k_{-GDP} = 0.002$ s^{-1} and $k_{-GTP} = 0.03$ s^{-1} (*23*)), which requires EF-Ts as the GEF, but consistent with EF-G ($k_{-GDP} = 300$ s^{-1} and $k_{-GTP} = 7$ s^{-1} (*21*)) which does not require a GEF for its cellular function. The kinetic data also suggest that HflX is in a constant state of nucleotide exchange in the cell similar to EF-G but opposed to EF-Tu (*22*, *23*). However, the rates of nucleotide dissociation from HflX are 1 order of magnitude lower than for the EF-Ts catalyzed nucleotide dissociation in EF-Tu (125 s^{-1} and 85 s^{-1} for GDP and GTP, respectively (*23*)). Furthermore, the rate constants governing the interaction between GTP and IF-2 ($k_{-GTP} = 15$ s^{-1} and $k_{+GTP} = 4 \times 10^5$ M^{-1} s^{-1} (*24*)) are very similar to HflX (Table 2). Interestingly, the association rate constants for the di- and trinucleotides binding to HflX differ significantly (Table 3), with k_1 (mant-GTP association) being much smaller than expected for a simple bimolecular association (in the order of 10^8 M^{-1} s^{-1} for a diffusion limited reaction), indicating that GTP binding to HflX requires a conformational change of the enzyme. These observations therefore imply different structures for the GDP- and GTP-bound states of HflX which is not surprising for a G-protein and is in agreement with the different FRET efficiencies observed in the mant-GTP and mant-GDP complexes of HflX (Figure 2C,D). However, the observation that the rates of nucleotide dissociation from both, the GDP- and GTP-bound complex were comparable seems to contradict different conformations for the GTP and the GDP state and would suggest a similar structure for the two complexes. It will be interesting to compare the GTP- and GDP-bound forms of HflX by structural studies.

The role of the ATP/ADP bound forms versus the GTP/GDP forms of the enzyme, if any exists, remains unclear since previous studies on the *E. coli* and the *C. pneumoniae* are not consistent with respect to a potential inhibition of the intrinsic GTPase by excess adenine nucleotides and vice versa (*9*, *10*). The observation that FRET from the tryptophans in HflX to the mant-group of mant-adenine nucleotides is less efficient than to the respective guanine nucleotides (as observed in both the equilibrium binding studies and pre-steady-state experiments) may be explained by either extremely slow association or dissociation rates, or an increased distance between the donor fluorophore (intrinsic tryptophan residues in HflX) and the acceptor fluorophore (mant-group) for the adenine compared to the guanine nucleotides. This would support the idea that the adenine-nucleotide bound state differs structurally from the guanine-nucleotide bound state, and may be part of a regulatory mechanism (*10*). However, based on the equilibrium dissociation constants reported here the majority of HflX will be bound to guanine nucleotides in vivo.

In this study, the use of a highly purified reconstituted translation system revealed for the first time that the GTPase activity of HflX is dramatically increased in the presence of 70S and poly(U)-programmed ribosomes and not only by 50S ribosomal subunits as previously reported (*10*). This finding suggests a functional interaction of HflX with the intact 70S ribosome, raising the question to what the functional role of HflX is and with which functional state of the ribosome it preferentially interacts. Previously, *E. coli* 70S ribosomes were not reported to interact with HflX nor to stimulate the GTPase activity of the protein (*10*). This may be explained by a lower affinity of *C. pneumonia* HflX for the *E. coli* 70S ribosomes used in the heterologous system or by the experimental conditions, for example, Mg^{2+} concentrations, which are not mimicking the cellular conditions. More importantly, the ribosome preparations used by Jain et al. are only partially purified and may still contain other factors such as mRNA, tRNA and translation factors which could influence the functional state of the ribosome

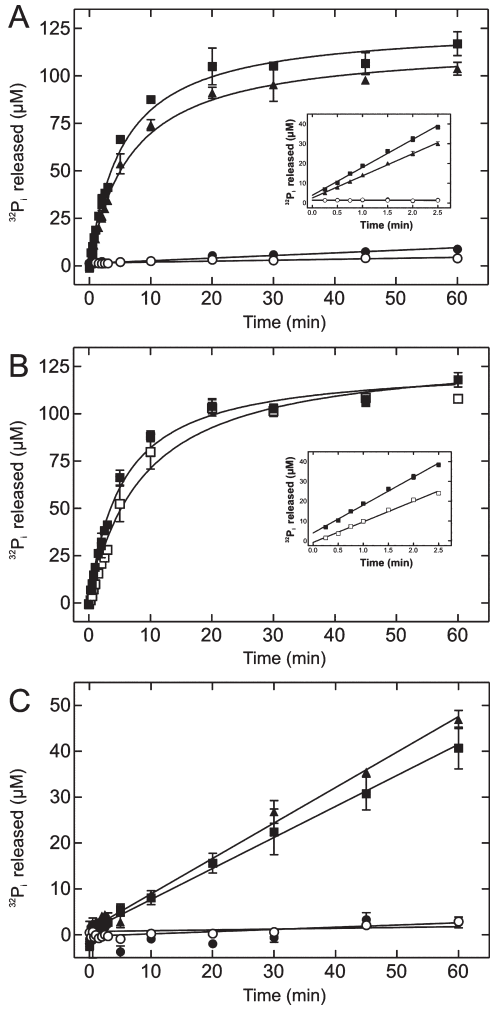

FIGURE 4: Ribosome-stimulated NTPase activity of HflX. (A) Time courses of GTP hydrolysis by HflX were obtained by extracting released $^{32}P_i$ and scintillation counting. The reaction was followed in the absence of ribosomes (open circles) or in the presence of 70S ribosomes (closed squares), 50S ribosomal subunits (closed triangles), and 30S ribosomal subunits (closed circles). The inset shows the initial phase of GTP hydrolysis. (B) Time courses of GTP hydrolysis by HflX in the presence of empty 70S ribosomes (closed squares) as well as ribosomes programmed with poly(U) as a mRNA message and the P-site occupied with $tRNA^{Phe}$ (open squares). Inset, same as in (A). (C) Time courses of ATP hydrolysis by HflX in the absence of ribosomes (open circles) or in the presence of 70S ribosomes (closed squares), 50S ribosomal subunits (closed triangles), and 30S ribosomal subunits (closed circles).

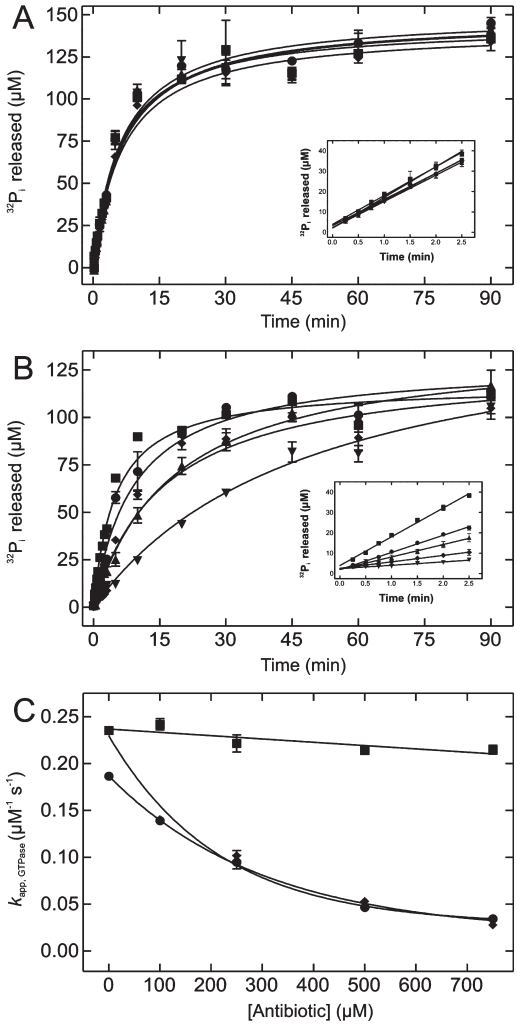

FIGURE 5: The ribosome-stimulated GTPase activity of HflX is inhibited by chloramphenicol but not by kanamycin. Time courses of GTP hydrolysis in the presence of increasing amounts of kanamycin (A) and chloramphenicol (B). The insets show the initial phase of GTP hydrolysis. Antibiotic concentrations: 0 μM, closed squares; 100 μM, closed circles; 250 μM, closed triangles; 500 μM, closed diamonds; 750 μM, reversed closed triangles. (C) Dependence of the apparent rate constant of GTP hydrolysis (k_{GTPase}) on the concentration of kanamycin (closed squares) and chloramphenicol (closed diamonds, 70S ribosomes; closed circles, 50S ribosomal subunits).

and hence the interaction with HflX. However, our own data using poly(U)-programmed, highly purified ribosomes with $tRNA^{Phe}$ in the ribosomal P site provided the same level of stimulation as observed for purified, empty ribosomes (Figure 4B). This demonstrates that the empty ribosome is not the only target of HflX, since the termination-like complex (70S-poly(U)-$tRNA^{Phe}$) is also recognized.

Chloramphenicol or the aminoglycoside kanamycin effectively inhibit protein synthesis (*15*−*17*, *33*, *34*). To explore a potential role of HflX during protein synthesis, we have examined the effect of these two antibiotics on the ribosome-stimulated GTPase activity of HflX. Chloramphenicol is a 50S subunit specific antibiotic with two binding sites on the prokaryotic ribosome: a high affinity (K_D = 2 μM) site near the ribosomal A site, which hampers binding of tRNA to the A site (*14*), and a lower affinity (K_D = 200 μM) site that binds to the peptide exit tunnel, which may inhibit nascent polypeptides leaving the tunnel (*35*). Chloramphenicol is toxic to prokaryotes but has little effect on eukaryotes, due to the lack of the higher affinity site (*34*−*36*). However, it has been suggested that both sites are physiologically important in bacteria, which further explains its potent antimicrobial activity (*36*). Our own data show an IC_{50} = 200 μM for the ribosome-stimulated GTPase activity of HflX. However, as the chloramphenicol binding sites on the 50S subunit and 70S ribosome are buried, this suggests the inhibition effect observed may be due to a conformational change near the chloramphenicol binding site affecting the HflX binding region, which in turn may influence the activity of the protein. This may hint at a previously unknown mechanism of antibiotic action through inhibition of the ribosome-associated activity of HflX. Kanamycin, in contrast, protects bases A1408, G1419, and G1494 on the 16S rRNA of the 30S subunit near the mRNA decoding center on the 70S ribosome (*15*−*17*) and does not show any effect on HflX's ribosome-dependent GTPase activity. Preliminary data suggests that hygromycin B, another

aminoglycoside that binds close to the decoding center on the ribosomal 30S subunit, also shows no effect on the ribosome-stimulated GTPase activity of HflX. Altogether this supports a model where HflX interacts with the 50S subunit of the ribosome which serves as a GTPase activating factor (GAP in analogy to the GTPase cycle) that is specifically inhibited by chloramphenicol.

In summary, we have presented the first detailed kinetic analysis of the nucleotide binding properties for the universally conserved GTPase HflX. On the basis of this, we were able to show that HflX exhibits a ribosome-stimulated GTPase activity, a feature also observed in several other ribosome-associated protein factors, including the canonical translation factors EF-Tu and EF-G. The use of a highly purified *E. coli* in vitro translation system allowed us to demonstrate that the ATPase activity of HflX is also stimulated by ribosomes. As a nonessential protein under optimal growth conditions, this factor may however have a role in protein synthesis or ribosome biogenesis under stress conditions. Our data on the antibiotic-dependent inhibition of the ribosome-stimulated GTPase activity point toward a role for HflX during protein synthesis, and suggests that the HflX-ribosome interaction may be a potential target for other antibiotics such as anisomycin, sparsomycin, blasticidin S, and virginiamycin M, which bind at the peptidyl transferase center of the 50S ribosomal subunit (*36*). Further kinetic analysis of HflX interaction with the ribosome, enabled through our current findings, as well as structural data on HflX along with identification of the ribosome binding site will be required in order to elucidate the precise function of HflX.

ACKNOWLEDGMENT

We thank Ute Kothe for critically reading the manuscript and for valuable suggestions. This work was supported by the National Science and Engineering Research Council of Canada, Canada Foundation for Innovation, and the Canadian Institutes for Health Research.

REFERENCES

1. Bourne, H. R., Sanders, D. A., and McCormick, F. (1991) The GTPase superfamily: conserved structure and molecular mechanism. *Nature 349*, 117–127.
2. Caldon, C. E., and March, P. E. (2003) Function of the universally conserved GTPases. *Curr. Opin. Microbiol. 6*, 135–139.
3. Brown, E. D. (2005) Conserved P-loop GTPases of unknown function in bacteria: an emerging and vital ensemble in bacterial physiology. *Biochem. Cell. Biol. 83*, 738–746.
4. Siderovski, D. P., and Willard, F. S. (2005) The GAPs, GEFs, and GDIs of heterotrimeric G- protein alpha subunits. *Int. J. Biol. Sci. 1*, 51–66.
5. Dovas, A., and Couchman, J. R. (2005) RhoGDI: multiple functions in the regulation of Rho family GTPase activities. *Biochem. J. 390*, 1–9.
6. Seabra, M. C., and Wasmeier, C. (2004) Controlling the location and activation of Rab GTPases. *Curr. Opin. Cell. Biol. 16*, 451–457.
7. Banuett, F., and Herskowitz, I. (1987) Identification of polypeptides encoded by an *Escherichia coli* locus (*hflA*) that governs the lysis-lysogeny decision of bacteriophage lambda. *J. Bacteriol. 169*, 4076–4085.
8. Noble, J. A., Innis, M. A., Koonin, E. V., Rudd, K. E., Banuett, F., and Herskowitz, I. (1993) The *Escherichia coli hflA* locus encodes a putative GTP-binding protein and two membrane proteins, one of which contains a protease-like domain. *Proc. Natl. Acad. Sci. U.S.A. 90*, 10866–10870.
9. Polkinghorne, A., Ziegler, U., Gonzalez-Hernandez, Y., Pospischil, A., Timms, P., and Vaughn, L. (2008) *Chlamydophila pneumoniae* HflX belongs to an uncharacterized family of conserved GTPases and associates with the *Escherichia coli* 50S large ribosomal subunit. *Microbiology 154*, 3537–3546.
10. Jain, N., Dhimole, N., Khan, A. R., De, D., Tomar, S. K., Sajish, M., Dutta, D., Parrack, P., and Prakash, B. (2009) *E. coli* HflX interacts with 50S ribosomal subunits in presence of nucleotides. *Biochem. Biophys. Res. Commun. 379*, 201–205.
11. Gradia, D. F., Rau, K., Umaki, A. C. S., deSouza, F. S. P., Probst, C. M., Correa, A., Holetz, F. B., Avila, A. R., Krieger, M. A., Goldenberg, S., and Fragoso, S. P. (2009) Characterization of a novel Obg-like ATPase in the protozoan *Trypanosoma cruzi*. *Int. J. Parasitol. 39*, 49–58.
12. Koller-Eichhorn, R., Marquardt, T., Gail, R., Wittinghofer, A., Kostrewa, D., Kutay, U., and Kambach, C. (2007) Human OLA1 defines an ATPase subfamily in the Obg family of GTP-binding proteins. *J. Biol. Chem. 282*, 19928–19937.
13. Dutta, D., Bandyopadhyay, K., Datta, A. B., Sardesai, A. A., and Parrack, P. (2009) Properties of HflX, an enigmatic protein from *Escherichia coli*. *J. Bacteriol. 191*, 2307–2314.
14. Schlunzen, F., Zarivach, R., Harms, J., Bashan, A., Tocilj, A., Albrecht, R., Yonath, A., and Franceschi, F. (2001) Structural basis for the interaction of antibiotics with the peptidyl transferase centre in eubacteria. *Nature 413*, 814–821.
15. Woodcock, J., Moazed, D., Cannon, M., Davies, J., and Noller, H. F. (1991) Interaction of antibiotics with A- and P-site-specific bases in 16S ribosomal RNA. *EMBO J. 10*, 3099–3103.
16. Moazed, D., and Noller, H. F. (1987) Interaction of antibiotics with functional sites in 16S ribosomal RNA. *Nature 327*, 389–394.
17. Jerinic, O., and Joseph, S. (2000) Conformational changes in the ribosome induced by translational miscoding agents. *J. Mol. Biol. 304*, 707–713.
18. Gasteiger, E., Hoogland, C., Gatiker, A., Duvaud, S., Wilkins, M. R., Appel, R. D., Bairoch, A. (2005) Protein identification and analysis tools on the ExPASy server, Springer-Verlag New York, LLC, New York, N.Y.
19. Rodnina, M. V., Fricke, R., and Wintermeyer, W. (1994) Transient conformational states of aminoacyl-tRNA during ribosome binding catalyzed by elongation factor Tu. *Biochemistry 33*, 12267–12275.
20. Watanabe, S. (1972) Interaction of siomycin with the acceptor site of *Escherichia coli* ribosomes. *J. Mol. Biol. 67*, 443–457.
21. Wilden, B., Savelsbergh, A., Rodnina, M. V., and Wintermeyer, W. (2006) Role and timing of GTP binding and hydrolysis during EF-G-dependent tRNA translocation on the ribosome. *Proc. Natl. Acad. Sci. U.S.A. 103*, 13670–13675.
22. Wieden, H. J., Gromadski, K., Rodnin, D., and Rodnina, M. V. (2002) Mechanism of elongation factor (EF)-Ts-catalyzed nucleotide exchange in EF-Tu. *J. Biol. Chem. 277*, 6032–6036.
23. Gromadski, K. B., Wieden, H. J., and Rodnina, M. V. (2002) Kinetic mechanism of elongation factor Ts-catalyzed nucleotide exchange in elongation factor Tu. *Biochemistry 41*, 162–169.
24. Milon, P., Tischenko, E., Tomsic, J., Caserta, E., Folkers, G., La Teana, A., Rodnina, M. V., Pon, C. L., Boelens, R., and Gualerzi, C. O. (2006) The nucleotide-binding site of bacterial translation initiation factor 2 (IF-2) as a metabolic sensor. *Proc. Natl. Acad. Sci. U.S.A. 103*, 13962–13967.
25. Leipe, D. D., Wolf, Y. I., Koonin, E. V., and Aravind, L. (2002) Classification and evolution of -loop GTPases and related ATPases. *J. Mol. Biol. 317*, 41–72.
26. Jiang, M., Datta, K., Walker, A., Strahler, J., Bagamasbad, P., Andrews, P. C., and Maddock, J. (2006) The *Escherichia coli* GTPase $CgtA_E$ is involved in late steps of large ribosome assembly. *J. Bacteriol. 188*, 6757–6770.
27. Sikora, A. E., Zielke, R., Datta, K., and Maddock, J. R. (2006) The *Vibrio harveyi* GTPase $CgtA_V$ is essential and is associated with the 50S ribosomal subunit. *J. Bacteriol. 188*, 1205–1210.
28. Neuhard, J., Nygaard, P. (1987) Purines and pyrimidines, Vol. 1, American Society for Microbiology, Washington, DC.
29. Buckstein, M. H., He, J., and Rubin, H. (2008) Characterization of nucleotide pools as a function of physiological state in *Escherichia coli*. *J. Bacteriol. 190*, 718–726.
30. Baba, T., Ara, T., Hasegawa, M., Takai, Y., Okumura, Y., Baba, M., Datsenko, K. A., Tomita, M., Wanner, B. L., Mori, H. (2006) Construction of *Escherichia coli* K-12 in-frame, single-gene knockout mutants: the Keio collection, Mol. Syst. Biol. doi:10.1038/msb4100050
31. Lin, B., Covalle, K. L., and Maddock, J. R. (1999) The *Caulobacter crescentus* CgtA protein displays unusual guanine nucleotide binding and exchange properties. *J. Bacteriol. 181*, 5825–5832.
32. Wout, P., Pu, K., Sullivan, S. M., Reese, V., Zhou, S., Lin, B., and Maddock, J. R. (2004) The *Escherichia coli* GTPase $CgtA_E$ cofractionates with the 50S ribosomal subunit and interacts with SpoT, a ppGpp synthetase/hydrolase. *J. Bacteriol. 186*, 5249–5257.

33. Brock, T. D. (1961) Chloramphenicol. *Bacteriol. Rev. 25*, 32–48.
34. Hobbie, S. N., Pfister, P., Brüll, C., Westhof, E., and Böttger, E. C. (2005) Analysis of the contribution of individual substituents in 4,6-aminoglycoside-ribosome interaction. *Antimicrob. Agents Chemother. 49*, 5112–5118.
35. Long, K. S., and Porse, B. T. (2003) A conserved chloramphenicol binding site at the entrance to the ribosomal peptide exit tunnel. *Nucleic Acids. Res. 31*, 7208–7215.
36. Hansen, J. L., Moore, P. B., and Steitz, T. A. (2003) Structures of five antibiotics bound at the peptidyl transferase center of the large ribosomal subunit. *J. Mol. Biol. 330*, 1061–1075.
37. Pon, C. L., Paci, M., Pawlik, R. T., and Gualerzi, C. O. (1985) Structure-function relationship in *Escherichia coli* initiation factors. biochemical and biophysical characterization of the interaction between IF-2 and guanosine nucleotides. *J. Biol. Chem. 260*, 8918–8924.
38. Peluso, P., Shan, S., Nock, S., Herschlag, D., and Walter, P. (2001) Role of SRP rNA in the GTPase cycles of Ffh and FtsY. *Biochemistry 40*, 15224–15233.
39. Lehoux, I. E., Mazzulla, M. J., Baker, A., and Petit, C. M. (2003) Purification and characterization of YihA, an essential GTP-binding protein from *Escherichia coli*. *Protein Expr. Purif. 30*, 203–209.
40. Teplyakov, A., Obmolova, G., Chu, S. Y., Toedt, J., Eisenstein, E., Howard, A. J., and Gilliland, G. L. (2003) Crystal structure of the YchF protein reveals binding sites for GTP and nucleic acid. *J. Bacteriol. 185*, 4031–4037.